JOURNAL OF Applied Polymer SCIENCE

Investigation of the physico-mechanical properties of electrospun PVDF/cellulose (nano)fibers

Ahmed A. Issa,[1] Mariam Al-Maadeed,[1,2] Adriaan S. Luyt,[2] Miroslav Mrlik,[2] Mohammad K. Hassan[2]
[1]Material Sciences and Technology Program, Qatar University, Doha, Qatar
[2]Center for Advanced Materials, Qatar University, Doha, Qatar
Correspondence to: A. S. Luyt (E-mail: aluyt@qu.edu.qa)

ABSTRACT: The electro-activity and mechanical properties of PVDF depends mainly on the β-phase content and degree of crystallinity. In this study, cellulose fibers were used to improve these characteristics. This could be achieved because the hydroxyl groups on cellulose would force the fluorine atoms in PVDF to be in the trans-conformation, and the cellulose particles could act as nucleation centers. Electrospinning was used to prepare the PVDF/cellulose (nano)fibrous films, and this improved the total crystallinity and the formation of β-crystals. However, the presence and amount of cellulose in PVDF were found to have little influence on the β-phase content and on the total crystallinity of PVDF. Improvements in the extent of crystallinity and the β-phase content were primarily brought about by the chain- and crystal orientation as a result of electrospinning. The thermal stability of PVDF in the composites slightly increased with increasing cellulose content in the composites up to 1.0 wt %, while the modulus and tensile strength significantly increased up to the same filler level. The dielectric storage permittivity also increased with increasing cellulose content, but the presence of cellulose had no influence on the dynamics of the γ- and β-relaxations of the PVDF. © 2016 Wiley Periodicals, Inc. J. Appl. Polym. Sci. **2016**, *133*, 43594.

KEYWORDS: composites; crystallization; differential scanning calorimetry (DSC); electrospinning; mechanical properties

Received 18 November 2015; accepted 2 March 2016
DOI: 10.1002/app.43594

INTRODUCTION

Poly(vinylidene difluoride) (PVDF) is a semicrystalline piezoelectric material with outstanding physical and mechanical properties, and it has been used in many fields, such as sensors, actuators, transducers, artificial muscles, energy storage, energy harvesting, water purification, and gas separation. It has the chemical structure $[—H_2C—CF_2—]_n$, and each monomer acts as a separate dipole due to the presence of two fluorine atoms (which has the highest electronegativity in the periodic table) in the vinylidene difluoride (VDF) repeat units of the polymer. The net dipole moment and direction of these dipoles are determined by the way of packing of these repeat units inside the polymer. It has three common phases (α, β, and γ).[1,2] The most common phase is the α-phase (TGTG), which is a nonelectroactive phase, where T refers to a trans and G to a gauche conformation, and it is the crystalline phase that normally forms when the polymer melt cools under ambient conditions. The electroactive phase is the β-phase (TTTT), where all the fluorine atoms are in the trans position. The polarity of the γ-phase (TTTGTTTG) is moderate between the α- and β-phases. The physical and mechanical properties of the polymer depend on the crystallinity and the phase.

The piezoelectricity of PVDF depends on the β-content and degree of crystallinity, and therefore most researchers worked on improving the β-phase content and crystallinity by using different techniques, such as mechanical stretching,[2] using additives or fillers,[3,4] electrical polling, different solvents during casting,[5,6] and electrospinning.[7]

In electrospinning, the (nano)fibers are formed under the influence of a high applied voltage, where the polymer melt or solution is driven from a metallic needle (spinneret) to a metallic collector under the flow rate and high voltage.[8,9] Researchers investigating the electrospinning of PVDF found the ideal PVDF concentration to be between 10 and 20 wt %, depending on the solvent used and the polymer molecular weight. Some added organic or inorganic salts to increase the conductivity of the electrospinning solution, which led to a reduction in the fiber diameters and an improvement in the β-phase content.[7,10] The β-phase content of PVDF can be improved by electrospinning due to the (i) shear force when the solution is ejected from the needle, (ii) electrostatic force between the spinneret and collector, (iii) mechanical stretching through polling of the fibers by a rotating drum.[7] However, it was found that the main reason for the molecular orientation to the β-phase is the

Table I. Electrospinning Conditions for PVDF

Parameter	Value
Concentration	13% w/w
Flow rate	3 mL h^{-1}
Voltage/temp.	10.35 kV/ambient
Needle	G20 (inner diameter $\geq$ 600 μm)
Distance	10 cm
Collector/speed	Drum with horizontal position of the needle/1400 rpm

electrostatic force, although the mechanical force was found to have an insignificant influence. Variation in the DMF:acetone solvent composition had no influence, probably because both are polar solvents.

Additives were also used to increase the β-phase content in the final product, and each filler has its own mechanism to do that, such as graphene oxide which improves the β-phase content through interaction between the electron-rich oxygenated groups and the fluorine atoms,[11] or cellulose which improves the β-phase content by interaction between the polar hydroxyl groups and the fluorine atoms in the PVDF molecule.[4,12] When polar solvents are used during PVDF processing, it can also lead to the formation of a β-phase.[13]

Investigation of cellulose in different forms (ball-milled, nanowhiskers, microcrystalline, alkali treated) to be used for the preferential nucleation of PVDF into the β-phase showed that the nanowhiskers were the most effective because of their large surface areas and the presence of —OH groups on the surface. Alkali treatment reduced this effect due to the interaction of sodium with the surface —OH groups. When comparing cellulose as additive with nanoclay and multiwalled carbon nanotubes (MWCNTs), it was found that the nanowhiskers compared well with the MWCNTs in preferentially nucleating the β-phase, and that both were better than the nanoclay. It was concluded that the β-phase nucleation was due to the presence of the —OH group rather than the preferential nucleation of the polymer chains on the additive surfaces.[4,12]

The main aim of this article was the preparation of (nano)fibrous PVDF films with high β-phase content and degree of crystallinity. Cellulose was used as a filler because of its availability in nature, its low cost, and the hydroxyl groups in its structure that could force the PVDF chains to crystallize into a β-configuration. The PVDF/cellulose (nano)fibrous mats were prepared through electrospinning from PVDF solutions in dimethyl formamide (DMF)/acetone containing different cellulose contents. The morphologies of the filler and the fibers were characterized by scanning electron microscopy (SEM). Crystallinity and β-phase formation were investigated using differential scanning calorimetry (DSC), Fourier-transform infrared (FTIR) spectroscopy, and X-ray diffractometry (XRD). The influence of the presence of cellulose and changes in the PVDF morphology on the thermal stability, mechanical properties, and dielectric properties were also investigated.

MATERIALS AND METHODS

All the reagents and chemicals used in this study were obtained commercially. PVDF in powder form (average molecular weight 534,000 amu determined by GPC, melting point 165 °C) from Sigma-Aldrich; acetone (ACS, 99.5+%) from Alfa Aesar; dimethyl formamide (DMF) (ACS, $\geq$99.8%) from Sigma Aldrich; cellulose (fiber, medium) from Sigma Aldrich.

Electrospinning Solution Preparation

Previous work by Refs. [4,7,12] was used as basis for the preparation of the electrospinning solution. After several trials, the following preparation method was found to give the best results: 60 g DMF, 40 g acetone, and 15 g PVDF were mixed and stirred under heating at 70 °C for 2 h until the solution was

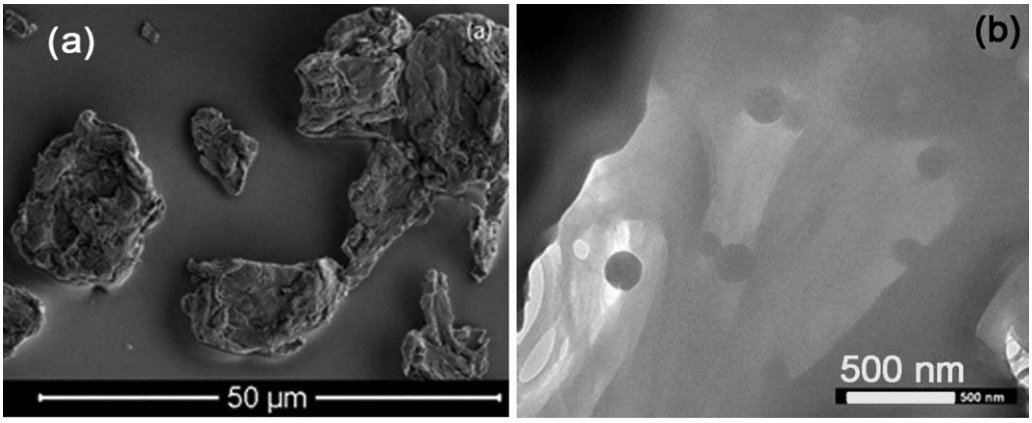

Figure 1. (a) SEM image of as-supplied cellulose and (b) TEM image of cellulose suspended in DMF/acetone/PVDF solution.

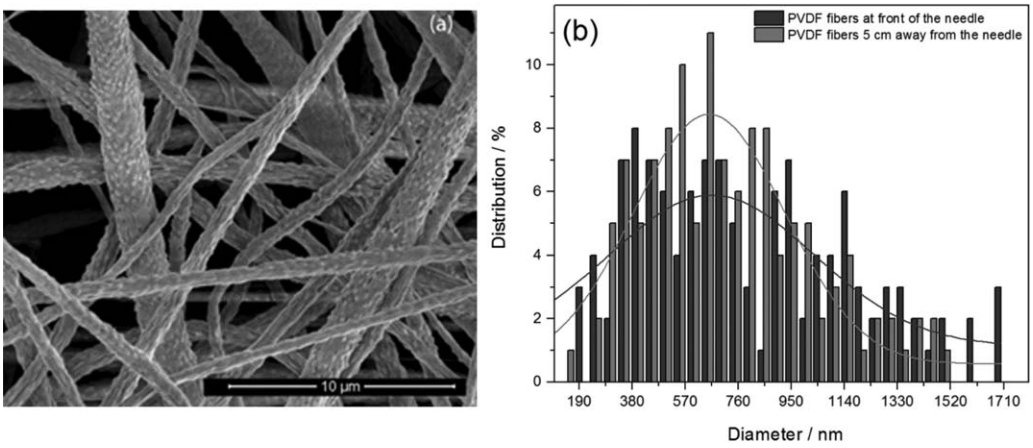

Figure 2. (a) SEM image of PVDF electrospun fibers and (b) distribution of electrospun fiber diameters.

clear. Cellulose (0.107 g) was then added to 20 g of this solution to give 4 wt % cellulose with respect to the amount of PVDF in the solution. Further dilutions with the PVDF solution were done to obtain solutions with different amounts of cellulose. Each sample was sonicated for 10 min before electrospinning.

Preparation of Electrospun Fibrous Mats

An electrospinning machine NEU-01 with its accessories from NaBond, China was used for the preparation of all the electrospun fibrous mats. The fabrication was carried out at room temperature and atmospheric pressure, using a standard G20 needle as the capillary. The fibrous mats were deposited on an aluminum foil covering a ground rotating drum. Each sample was electrospun until at least 4 mL of the solution was converted to a fibrous mat. The optimum conditions, obtained after experimenting with different variable combinations, are listed in Table I.

Characterization and Analysis Techniques

DSC analyses were performed on a Perkin Elmer DSC4000 differential scanning calorimeter. The samples were scanned in two cycles at a heating rate of 10 °C min^{-1}, from 40 to 200 °C in nitrogen.

The TGA analyses of the samples were done in a Perkin Elmer TGA4000 thermogravimetric analyzer from 40 to 750 °C at a constant heating rate of 10 °C min^{-1} in nitrogen gas.

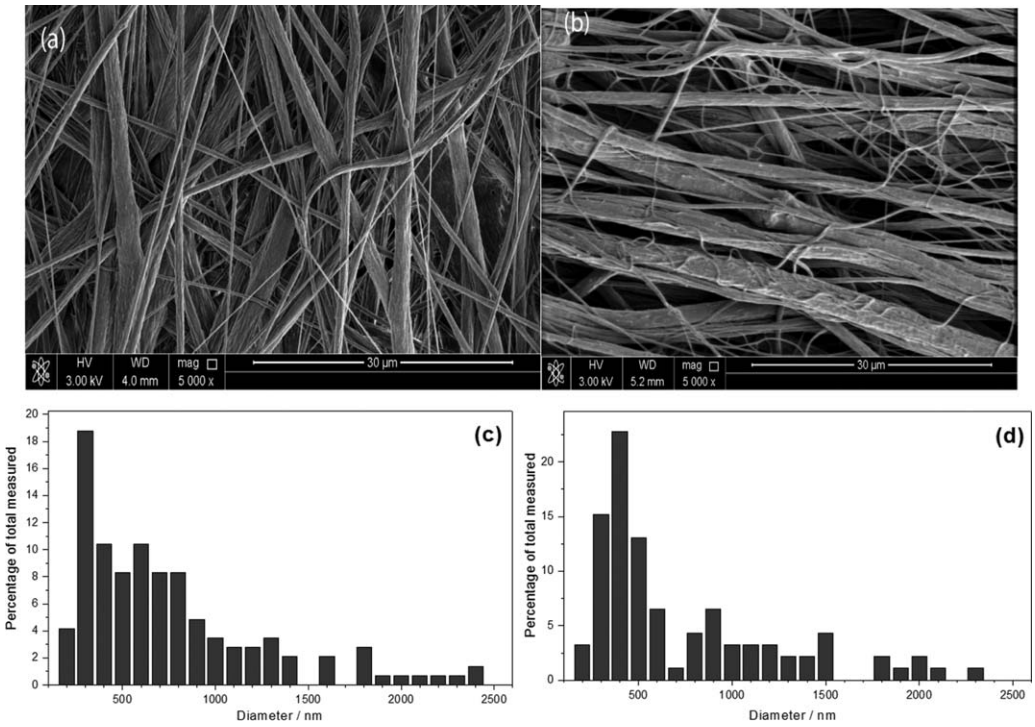

Figure 3. Selected SEM images of electrospun mats of PVDF with 2% cellulose collected by (a) drum and (b) rotating disk. Distribution of diameters of fibers collected by (c) drum and (d) rotating disk.

SEM analyses were done on an FEI Quanta 200, USA scanning electron microscope at an accelerating voltage of 3 kV. The ZEN imaging software from Zeiss was used to determine particle sizes and fiber diameters.

TEM analyses to examine the morphology of the cellulose filler were done on an FEI G2 TF20, USA transmission electron microscope by using an accelerating voltage of 200 kV.

Fourier-transform infrared (FTIR) spectroscopic analysis of the samples was done from 400 to 4000 cm^{-1} in a Perkin Elmer Spectrum 400 FTIR with an ATR detector at a resolution of 4 cm^{-1}.

XRD analyses were done on a Rigaku Minflix X-ray diffractometer with a Cu-K_α (1.5406 Å) source, applied voltage of 30 kV, current of 30 mA, and a scan rate of 3° min^{-1}.

A Lloyd Instruments LF Plus universal tester was used to measure the tensile strength of the (nano)fibrous films at room temperature. The samples were prepared with length 75 mm, width 5 mm, and thickness from 0.08 to 0.15 mm. The tests were conducted with a cross-head speed of 50 mm min^{-1} with a gauge length of 25 mm.

A TA Instruments RSA-G2 dynamic mechanical analyzer (DMA) was used to determine the G' and G''. The moduli were determined in the LVR which was established at a strain deformation of $\gamma = 0.008\%$ in a broad frequency range from 0.01 to 100 Hz. The measured samples were in the shape of strips with 40 mm in length, 3.5 mm in width, and a similar thickness range as was mentioned in the case of tensile testing. All the measurements were performed at room temperature.

Dielectric measurements were performed using a Novocontrol GmbH Concept 40 broadband dielectric spectrometer, and the data were collected over the frequency range 0.07 to 10^7 Hz at fixed temperatures in the range of −140 to 140 °C. The temperature stability of the instrument was within ±0.2 °C. Sample discs of 2 cm diameter were sandwiched between two gold-coated copper electrodes of 2 cm diameter, and transferred to the instrument for data collection.

RESULTS AND DISCUSSION

Morphology

Figure 1(a) shows the SEM image of the as-supplied cellulose filler; it shows the cellulose particles have irregular shapes with different sizes which ranged between 1 and 40 μm, with most of the particle sizes between 1 and 10 μm. The sizes are, however, too big to be incorporated in the fibers through electrospinning, and therefore, TEM analysis was done on the cellulose suspended in the DMF/acetone/PFDV solution [Figure 1(b)]. The TEM image shows nanosized particles in the gel-like solution used for the electrospinning. It does seem as if the cellulose formed a gel in the DMF/acetone solution with the most crystalline cellulose particles dispersed in this gel. This is a realistic possibility in view of the findings by Kamide *et al.*[14]

The PVDF electrospun (nano)fibrous mats were prepared with optimized conditions as in Table I, and with a concentration of 13 wt % of PVDF. The fibers were nonwoven, nonaligned, no beads were formed, and they had diameters varying between 370 and 870 nm [Figure 2(a)]. The thickness of the electrospun mats was not uniform, and it was observed to be thick and dense at the front of the spinneret (needle), and it became thinner away from the needle [Figure 2(b)]. It was found that the most critical parameter in the electrospinning process was the type of solvent because it (i) determined the dependence of the viscosity on the concentration of the electrospinning solution and (ii) controlled the solidification step of the (nano)fibers. Other research groups used different solvents that varied from pure DMF and dimethylacetamide (DMAc) to mixtures of DMF and acetone, or DMAc and acetone, with different ratios.[10,14,15] In this work, a DMF/acetone mixture was used to control the evaporation during the electrospinning.

Figure 2(a) shows that the fiber surfaces were not smooth, but rough and porous. This was due to the use of two different solvents in the solution, acetone (which has a boiling point of 56 °C) and DMF (which has a boiling point of 152 °C), that evaporated at different temperatures during electrospinning, and this caused the formation of the observed porous structure. It can also be observed that the thick fibers had a more porous and rough surface than the thin fibers because the thick fibers could trap the solvent for a longer time. Generally, a single solvent gives smooth fibers,[14] but mixtures of solvents give fibers with porous surfaces, especially when the difference in boiling points is large.[16] However, some research groups did use a mixture of solvents (e.g., DMAc and acetone) and still obtained smooth fibers.[10] The porosity of the fibers is an advantage, especially in (nano)fiber membranes, because it will increase the surface area.

Figure 2(b) shows the relation between the distribution of fiber diameters and the collected fibers' location (with respect to the needle position). It shows that the average diameter of the fibers at the front of the needle is 600 nm, while that of the fibers that were 5 cm away from the needle position is thicker and less dispersed, which means that the collected fibers further away from the needle position will be thinner. This is due to the fibers having more time to elongate, and for the solvent to evaporate.[10]

Figure 3 shows that the electrospun fibers collected on the rotating disk were more aligned than the fibers collected on the drum. The fiber diameter distribution curves in this figure show that the diameters of most of the fibers were below 1000 nm, and that the maximum probability diameter was lower for the fibers collected on the drum, which is to be expected because of the larger area of the drum which gives the fibers more time to be stretched. The SEM images (not shown here) of the fiber mats with different cellulose contents collected on the rotating disk show that they became more cylindrical with increasing the concentration of the cellulose. The diameters of the produced (nano)fibers decreased with increasing the concentration of cellulose. The enhancement of the fiber morphology could be due to the absorption of the solvents (specially the DMF) by the cellulose particles, which led to well-defined fibers. The swelling power of the cellulose to DMF and acetone are 62 and <15 (g/g), respectively.[17] The fiber shape and diameter depended on the conductivity of the

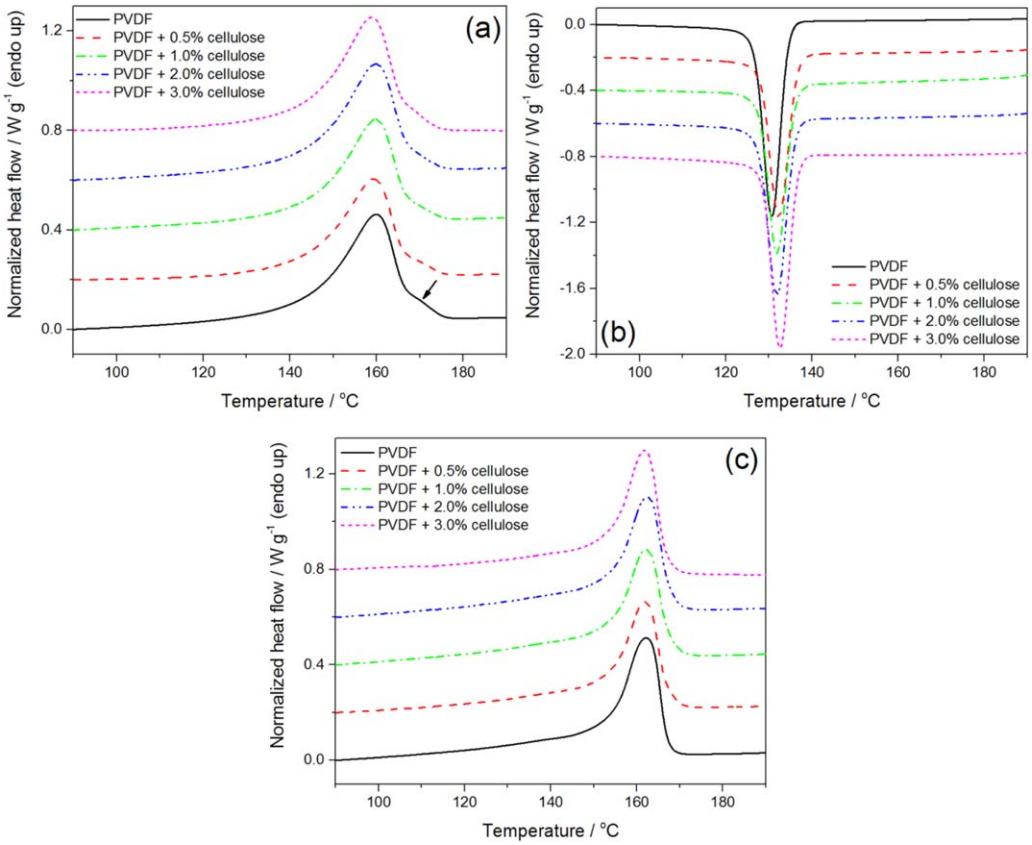

Figure 4. DSC curves of electrospun PVDF/cellulose fibers. [Color figure can be viewed in the online issue, which is available at wileyonlinelibrary.com.]

solution, and in this case, the swelling power of the cellulose and changes in the solution conductivity as a result of the cellulose charge content may have contributed to the reduced fiber diameter.

Crystallinity

A number of articles refer to the DSC technique as a complementary technique for FTIR and XRD in the identification of polymer phases,[18,19] because it does not depend on the PVDF phases only, but also on the crystal defects, that are affected by the processing conditions and filler additives. The melting point of the β- and α-phases is between 167 and 172 °C, that of the γ-phase between 179 and 180 °C, and that of the γ'-phase between 189 and 190 °C.[1] These values change with polymer molecular weight; in the case of PVDF with an average molecular weight (250,000 amu), the melting point varies between 156 and 160 °C, depending on the processing parameters.[7]

Figure 4 shows the DSC curves of PVDF and the PVDF/cellulose composites. The melting points of the first heating cycle are almost identical (around 160 °C), regardless of the cellulose content, and the same behavior was observed for the second heating cycle (around 162 °C). There is a difference of about 2 °C between the melting temperatures observed in the first and second heating cycles, probably because the controlled cooling in the DSC gave rise to larger crystals that melted at higher temperatures than the crystals formed during electrospinning. The crystallization temperatures for the cellulose-containing samples were slightly higher than that of pure PVDF, but did not change significantly with cellulose content in the samples

Table II. Normalized Enthalpies and Degrees of Crystallinity of PVDF in the PVDF/Cellulose Electrospun Fibers

Cellulose content/wt. %	ΔH^n_{m1} (J g^{-1})	χ_{m1} (%)	ΔH^n_c (J g^{-1})	χ_c (%)	ΔH^n_{m2} (J g^{-1})	χ_{m2} (%)
0	44.1	42.2	−35.9	34.3	34.8	33.3
0.5	42.5	40.6	−32.1	30.7	33.4	31.9
1	41.6	39.8	−34.4	32.9	33.6	32.1
2	46.7	44.7	−35.3	33.8	34.7	33.2
4	44.6	42.6	−37.4	35.8	36.1	34.5

ΔH^n_{m1}, ΔH^n_{m2}, and ΔH^n_c are the enthalpies normalized with respect to the PVDF content in the first heating, cooling, and second heating cycles, respectively. χ_{m1}, χ_c, *and* χ_{m2} are the degrees of crystallinity of PVDF calculated from the respective normalized enthalpies, using 104.6 J g^{-1} as the enthalpy of 100% crystalline PVDF.[4]

Table III. Characteristic FTIR Wavenumbers for Each Phase of PVDF [1,20–23]

	α-phase	β-phase	γ-phase
Wavenumbers/cm−1	408 (CF_2 rocking)	510 (CF_2 deformation)	431 (CF_2 rocking)
	532 (CF_2 deformation)	840 (CH_2 rocking)	512 (CF_2 deformation)
	614 (CF_2 wagging)	1279(CF_2 asym. stretch)	776 (CF_2 deformation)
	766 (CF_2 deformation)	485(CF_2 deformation)	812 (CH_2 rocking)
	795(CH_2 rocking)	440(CF_2 rocking)	833 (CH_2 rocking)
	855 (C-C sym. stretch)		840 (CH_2 rocking)
	976 (CH_2 twisting)		1234 (CF_2 asym. stretch)

[Figure 4(c)]. The higher temperature peak shoulder [arrow in Figure 4(a)] indicates that the electrospun fibers contained more than one crystalline structure, probably the α- and β-phases. The presence of the β-phase is due to (i) the cellulose particles serving as nucleating agents during the crystallization and (ii) the electrospinning process which forces the polymer chains to align in ordered structures. The latter is clear from the melting enthalpies (or crystallinities) of the electrospun fibers (Table II), where the first heating melting enthalpies were generally significantly higher than those observed during the second heating. The electrospun fiber that melted during the first heating cycle clearly had a much higher crystallinity than the solid polymer formed during controlled cooling in the DSC, which melted during the second heating cycle. The presence of cellulose did not have a significant influence on the melting enthalpies (or total crystallinities), which means that the increase in crystallinity was due to the electrospinning process and not to the presence of cellulose.

β-Phase Content

Researchers who previously studied the FTIR spectra of PVDF, assigned the bands at 3027 and 2986 cm^{-1} to the asymmetric and symmetric C—H stretching and those at 1456, 1405, 976, and 845 cm^{-1} to the bending, wagging, twisting, and rocking of the CH_2 group. The bands at 1074, 1026, and 880 cm^{-1} were assigned to the asymmetric and symmetric stretching of C—C, while those at 1212, 1184, 766, 612, and 435 cm^{-1} were assigned to the asymmetric, symmetric, deformation, wagging, and rocking modes of —CF_2.[20,21] Nowadays researchers use the FTIR fingerprint region (1500–400 cm^{-1}) to investigate the presence of the β-phase. However, the conformation of the β-phase is similar to that of the γ-phase, which causes some confusion because most of the β-phase bands are very close to those of the γ-phase as shown in Table III.

Table III shows the characteristic wavenumbers for each crystal phase of PVDF, and Figure 5 shows the relation between the β-phase content, calculated by using eq. (1),[2] and the concentration of cellulose.

$$\beta\text{-phase content } (\%) = \frac{A_{840}}{(1.26\ xA_{763} + A_{840})} \times 100 \qquad (1)$$

where A_{840} is the FTIR absorbance for the α-phase peak at 840 cm^{-1}, and A_{763} is the FTIR absorbance for the β-phase peak at 763 cm^{-1}. The β-phase content was approximately the same for the neat electrospun PVDF and the PVDF samples containing different amounts of cellulose. This clearly indicates that cellulose had very little influence on the β-crystal formation in PVDF during electrospinning. Another group, who prepared their samples through solution casting of PVDF containing uniform rod-like cellulose, observed a maximum for the β-phase content for the sample containing 1% of the filler.[11] In their case, the filler clearly had an influence on the formation of β-crystals, probably because they used a different sample preparation technique. The improvement in β-phase content would be due to the presence of —OH groups that strongly interact with the fluorine on the PVDF chains. This interaction would force the PVDF chains to rearrange into a trans-configuration where the fluorine atoms are on the same side of the chain, which is characteristic of the β-phase. In our case, this rearrangement seems to result from chain alignment during electrospinning, while the presence of cellulose has little effect.

The peaks that characterize each phase of PVDF in the XRD spectrum are listed in Table IV. Most of these peaks are around 20°, so it is difficult to use XRD alone to investigate the PVDF phases; it is usually used in combination with FTIR. The 2θ values are used interchangeably between the γ- and α-phases in the region 19.9–20.5°, which can lead to some confusion. The preparation technique has a direct effect, not only on the phase content but also on the compactness. Two samples were prepared from pure PVDF, one with a drum and the other with a rotating disk (RD)

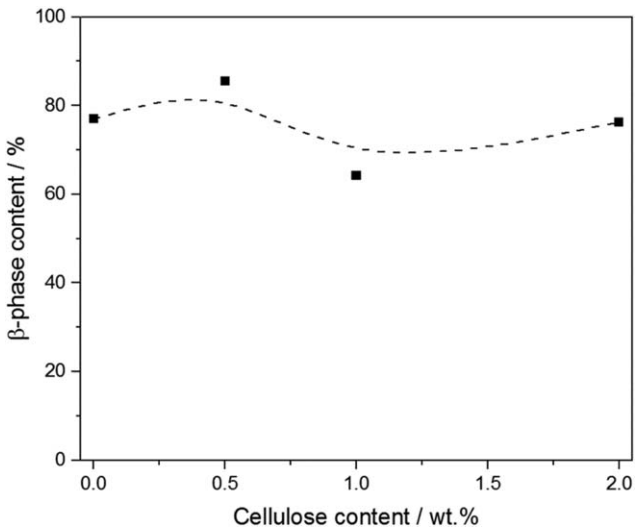

Figure 5. β-phase content in electrospun PVDF/cellulose composites.

Table IV. The 2θ Values for the Characteristic Peaks of the α-, β-, and γ-Phases of PVDF [1,24]

	α-phase	β-phase	γ-phase
2θ (°)	17.7	20.3	18.5
	18.3		19.2
	19.9		20.0
	26.6		26.8
	39.5		
Unit cell	Monoclinic ($a = 8.58$ Å, $b = 4.91$ Å, $c = 2.56$ Å)	Orthorhombic ($a = 4.96$ Å, $b = 9.64$ Å, $c = 4.62$ Å)	Monoclinic ($a = 8.66$ Å, $b = 4.93$ Å, $c = 2.58$ Å)

as collectors, and both of them contained β-phase crystals. The value of 2θ in the sample prepared by using the drum is lower than that for the sample prepared by using the rotating disk (Figure 6). According to the equation $n\lambda = 2d \sin\theta$, a decrease in 2θ is indicative of an increase in the internal distance d, so the crystals were less compact for the fiber collected on the drum.

Figure 7 shows the XRD spectra of the PVDF/cellulose electrospun fibers. There is no trend in the dependence of the peak intensities around 20° on the amount of fiber in the samples, and therefore, no conclusion can be drawn from the XRD results on β-crystal formation in these samples.

Thermal Stability

PVDF lost about 59% of its initial mass at the end of the first mass loss step (Figure 8), which corresponds to the loss of two molecules of HF, where the percentage of HF was calculated theoretically by using eq. (2).

$$w_{HF}\ \% = \frac{W_{HF}}{W_{VDF}}\ x\ 100 \qquad (2)$$

where w_{HF} % is the mass percentage of HF in the vinylidene fluoride molecule, w_{HF} is the molecular weight of the HF equal to 20 g mol^{-1}, and W_{VDF} is the molecular weight of the vinylidene fluoride molecule equal to 64 g mol^{-1}. So $2(w_{HF}\ \%) = \frac{2 \times 20}{64} \times 100 = 62.5\%$. Botelho *et al.*[25] studied the mechanism of thermal degradation of PVDF by using UV spectrometry linked to TGA, and they obtained similar results. The mass loss step above 500 °C is probably due to the degradation of the main chain in PVDF, and this is a slow process which is not yet completed at 700 °C. The release of HF is accompanied by carbonization of the polymer,[26] followed by cyclization of the species evolved. Polymer cross-linking occurs at higher temperatures, resulting in a fully carbonized residue. Cellulose shows three decomposition steps (Figure 8). The first is due to the loss of moisture and the formation of anhydrocellulose, while the second is the depolymerization of cellulose and the formation of char, while the third is a slow exothermic

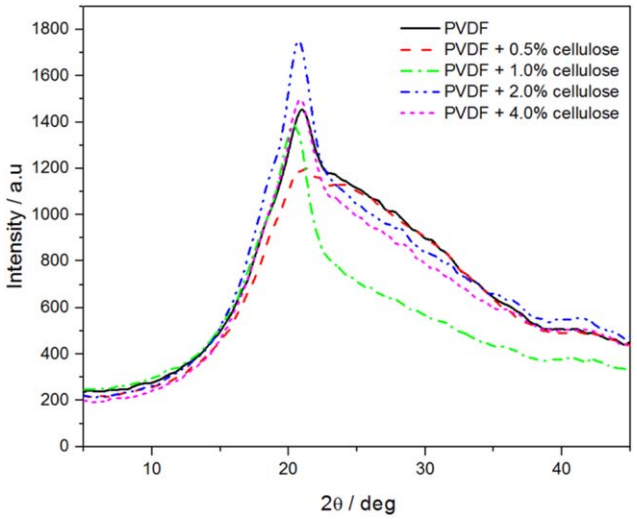

Figure 7. XRD spectra of dense electrospun films collected by rotating disk. [Color figure can be viewed in the online issue, which is available at wileyonlinelibrary.com.]

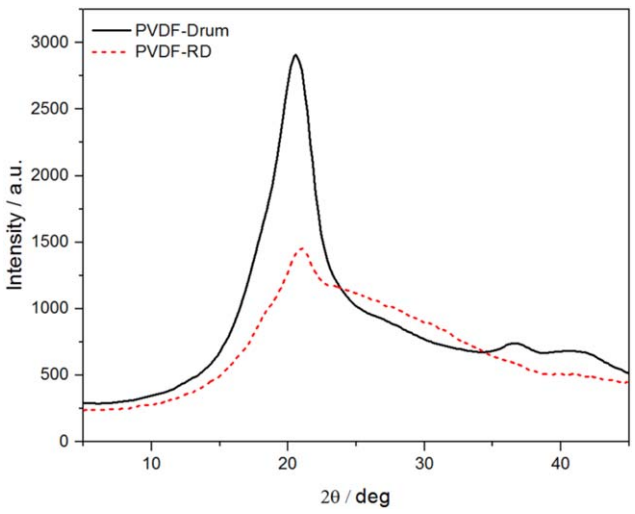

Figure 6. XRD spectra of dense electrospun films collected by drum and rotating disk (RD). [Color figure can be viewed in the online issue, which is available at wileyonlinelibrary.com.]

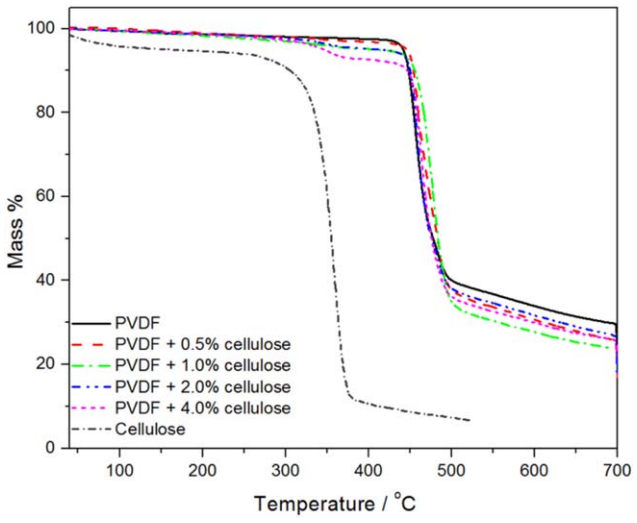

Figure 8. TGA curves of PVDF, cellulose, and different PVDF/cellulose composites. [Color figure can be viewed in the online issue, which is available at wileyonlinelibrary.com.]

Table V. Thermal Decomposition Temperature Regions

Temperature (°C)	Degradation products	References
<100	Crystalline water in the cellulose filler	26,27
150	Water due to dehydration of cellulose	26,27
350	Tar due to decomposition of anhydrocellulose	26,27
450	Hydrogen fluoride (HF) due to decomposition of PVDF	25
>550	Remaining char	25–27

decomposition of the formed char.[26,27] The composite samples show three decomposition steps, corresponding to loss of moisture below 200 °C, the decomposition of cellulose around 350 °C, and the decomposition of PVDF above 464 °C (Table V). The samples with cellulose concentrations of 0, 0.5, 2, and 4%, respectively, show weight losses of 3, 3.5, 5, and 7%. In each case, the difference is about 3%, which probably is the result of moisture trapped in the composite samples.

The temperatures at 30% mass loss in Table VI show an initial increase in thermal stability when cellulose was present in the electrospun PVDF, with the 1% cellulose containing sample having the highest thermal stability. This was probably due to char formation during the decomposition of the cellulose particles,[28] which could adsorb the volatile HF that formed during PVDF decomposition and only release it at higher temperatures.[29] The decomposition of cellulose at higher contents probably resulted in a change in the size and distribution of the char residue, which then reduced its effectiveness in delaying the diffusion of HF out of the sample and again decreased the temperature at 30% mass loss. It is, however, important to note that the mass loss between 450 and 500 °C occurs over a narrow temperature range, with the start and end of this step for the different samples being at almost the same temperatures. Small differences in the decomposition route between the different samples could therefore influence the shape of the curve during this decomposition step.

Mechanical Properties

Figure 9 shows that the tensile strength increased significantly with increasing cellulose content up to 1% cellulose content, and it remained constant for higher cellulose contents. Researchers who used PVDF to improve the mechanical properties of cellulose film, found that (i) the PVDF content should be <20% to give better improvement, (ii) as the amount of PVDF increased, the tensile strength decreased, and (iii) pure PVDF had a very low tensile strength of about 2 MPa, and for 20% PVDF/cellulose, it was 3 MPa.[30] The pure PVDF in our case already had a high tensile strength of more than 5 MPa, which was due to the higher crystallinity of and crystal orientation in the electrospun fibers. The presence of 1% and 2% cellulose almost doubled this value, which was probably due to strong hydrogen-bonding interactions between the fluorine atoms on the PVDF chains and the OH groups in cellulose.

Table VI. Temperatures at 30% Mass Loss for the PVDF/Cellulose Composites

Cellulose content (%)	0	0.5	1	2	4
T (°C)	459.7	466.2	473.0	460.8	463.5

Dynamic Mechanical Analysis (DMA)

Figure 10(a) shows that the storage modulus at all the investigated frequencies increased with increasing filler content, and that there was a significant improvement at a concentration of 0.5% cellulose. Since the presence of cellulose did not contribute to β-crystal formation in the electrospun fibers, and since there seems to be very little interaction between PVDF and the cellulose particles (as will be shown in the discussion of the dielectric properties of the investigated systems), this increase in storage modulus can only be explained as being the result of the presence of increasing amounts of cellulose with a higher inherent stiffness than PVDF. There was no optimum loading, and the G'' also increased with increasing cellulose content [Figure 10(b)].

Broadband Dielectric Analysis

Modern broadband dielectric spectroscopy (BDS) is commonly used to analyze materials' response over a wide frequency (f) (0.07–10^7 Hz) and temperature (T) window. BDS is therefore a very powerful tool for examining molecular dynamics and electrical polarizability of polymers over broad temperature and time scales.[31]

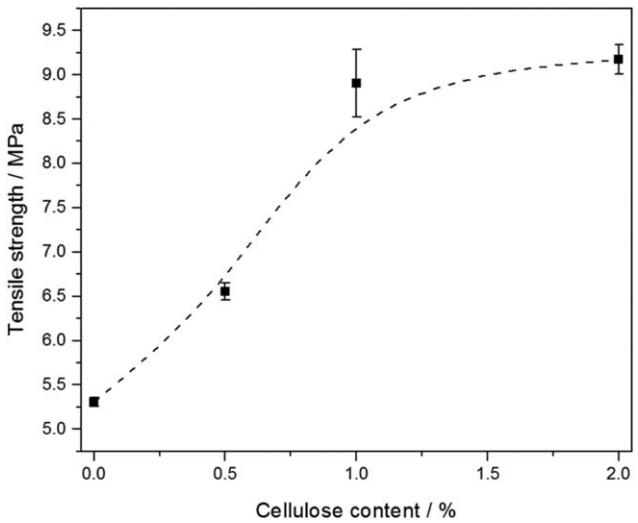

Figure 9. Tensile strengths of electrospun PVDF/cellulose composites with different cellulose contents.

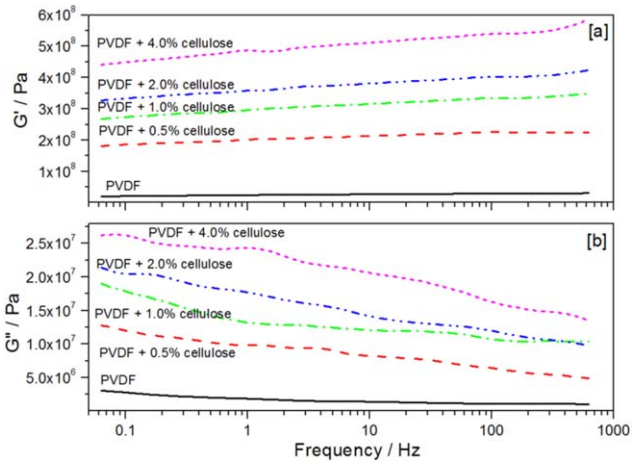

Figure 10. DMA results for the electrospun PVDF/cellulose samples: (a) storage modulus and (b) loss modulus. [Color figure can be viewed in the online issue, which is available at wileyonlinelibrary.com.]

In this section, we will examine the effect of cellulose on the electric polarizability and chain motions of the PVDF electrospun composites. Figure 11 shows the signatures of the control PVDF relaxations as crests on the 3D dielectric permittivity loss (ε'') $-f-T$ response surfaces, over a broad range of temperatures (-140 to 140 °C). Of interest herein is the β-relaxation peak, which has an onset temperature of approximately -80 °C and its crest shifted to higher frequencies with increasing temperatures in the usual non-Arrhenius fashion. The β relaxation is assigned to the long-range segmental mobility associated with the movement of chain segments within the crystalline–amorphous interphase.[32–35] Other researchers attributed this relaxation to micro-Brownian motions of amorphous phase chain segments.[36]

A detailed picture of the relaxation peaks in the low-temperature region is shown in the ε'' vs. temperature curves (Figure 12). Comparison was made at 1 Hz and 1 kHz to more clearly show the trends of the β and γ relaxation peak maxima.

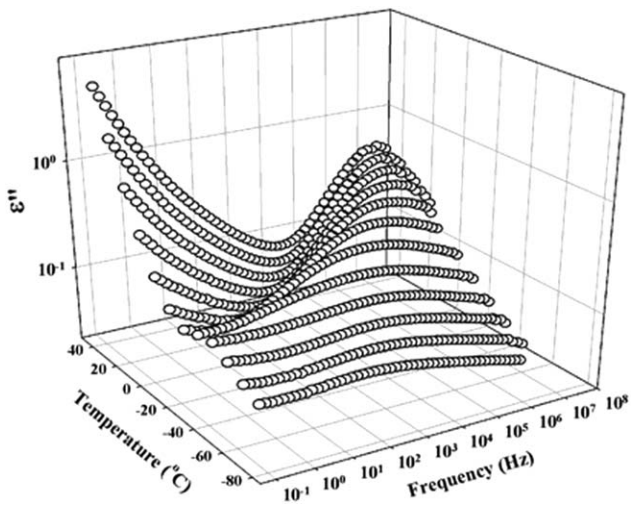

Figure 11. $\varepsilon'' - f - T$ surfaces for the control electrospun PVDF sample. Curves are spaced at 10 °C increments with onset of -80 °C showing the β-relaxation peak.

The γ-relaxation appears only when a comparison is made at 1 Hz. At this frequency, the time scale of the experiment is 1000 times longer than at 1 kHz, so that slow motions are more effectively captured. γ-relaxation is assigned to the local molecular motion in the amorphous region.[37] Dispersion of cellulose in the electrospun PVDF did not seem to alter the relaxation times of both the local and crystalline–amorphous interphase motions of the chains, as the γ- and β-relaxation peak maxima appear to have the same frequency for all the samples.

To further investigate the effect of cellulose dispersion on the β-relaxation of the electrospun PVDF, the ε'' vs. frequency spectra at different temperatures were fitted to the widely used Havriliak Negami (HN) equation[38,39] as shown in Figure 13. The frequency at the ε'' peak maximum, f_{max}, for the β-relaxation increases with increasing T, which indicates faster molecular motions and shorter relaxation times, $\tau_{max} = 1/2\pi\ f_{max}$, in the usual manner. The solid lines represent the HN model fits to the spectra and they all seem to have very good fits to this model. The relaxation times values were extracted from the fitted spectra at each temperature and then plotted against $1/T$ in Figure 14, showing non-Arrhenius behavior according to the Vogel–Fulcher–Tammann–Hesse (VFTH) equation [eq. (3)].[40]

$$\tau_{max}(T) = \tau_0 \exp\left(\frac{E_a}{k_B(T - T_V)}\right) \tag{3}$$

where k_B is the Boltzmann constant and τ_0 is the hypothetical relaxation time at infinite temperature. E_a has the units of energy, but is a ubiquitous quantity that it is not associated with an activated process in the normal sense. T_V, the Vogel temperature, is the temperature at which chain segments become frozen when the polymer is cooled quasi-statically from the rubbery state, in a hypothetical situation.

The curvature (as against linearity) of the VFTH equation fit, the dashed line in Figure 14, is distinctive of long-range motions in glass forming polymers. The relaxation times for the composite samples do not show any significant vertical shift relative to the control PVDF. This result reveals similar chain segmental motions within the crystalline–amorphous interphase, even after inclusion of the cellulose. The reason for the data scattering for the PVDF/cellulose samples below -35 °C is not quite clear to us at this point, but it could be due to interactions between the hydroxyl groups in cellulose and the fluorine groups along the PVDF chains.

The distribution of relaxation times, $G(\tau)$, is another representation that was used to further illustrate the behavior of the β-relaxation motion for the samples. $G(\tau)$ was constructed based on the relaxation peak asymmetry parameters, α and β, extracted from the Havriliak–Negami equation [eq. (4)] fitting of the spectra.[39]

$$G(\tau) = \frac{\left(\frac{\tau}{\tau_{0i}}\right)^{\beta_i\alpha_i} \sin(\beta_i\Theta_i)}{\pi\tau\left(\left(\frac{\tau}{\tau_{0i}}\right)^{2\alpha_i} + 2\left(\frac{\tau}{\tau_{0i}}\right)^{\alpha_i}\cos(\pi\alpha_i) + 1\right)^{\frac{\beta_i}{2}}} \tag{4}$$

$$\Theta_i = \arctan\left(\frac{\sin(\pi\alpha_1)}{\left(\frac{\tau}{\tau_{0i}}\right)^{\alpha_i} + \cos(\pi\alpha_1)}\right) \tag{5}$$

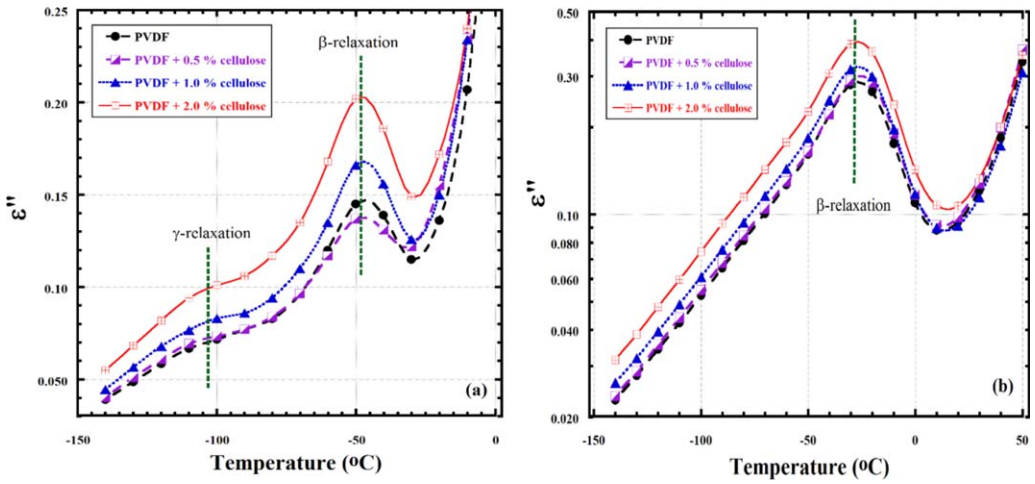

Figure 12. ε'' vs. temperature at (a) 0.1 Hz and (b) 1 kHz to show relaxation peaks in the low temperature region for the control and PVDF/cellulose electrospun composite samples. Dashed lines are used to show the γ- and β-relaxation peak maxima. [Color figure can be viewed in the online issue, which is available at wileyonlinelibrary.com.]

where α characterizes the peak breadth and β, by its deviation from unity, characterizes the degree of curve asymmetry. The angular quantity Θ_i has units of radians such that $0 \leq \Theta_i \leq \pi$.

The $G(\tau)$ plots at $-50\,^{\circ}C$ for the electrospun PVDF/cellulose samples are shown in Figure 15. Broad unimodal curves are evident for all the samples. The $G(\tau)$ curves have similar maxima at a relaxation time of $\cong 10^{-4}$ (sec) which confirms the above-mentioned conclusion that cellulose insertion did not disturb the long-range chain segmental mobility within the crystalline–amorphous interphase.

The broadness of the β-transition could be explained in terms of the fact that this relaxation is complex and arises from at least two contributions, namely motions within the crystal–amorphous interphase and a transition accounting for the non-constrained segments movement in the amorphous phase.[41] The latter would be responsible for the small shoulder which appears at the low relaxation time side of the $G(\tau)$ peak for the 1% cellulose sample.

The frequency dependence of the dielectric permittivity storage (ε') and loss (ε'') at 20 °C for the composites is shown in Figure 16. Increasing the cellulose content rendered the composite more polarizable, as indicated by the increase in ε' values with an increase in the filler loading. One possible explanation is that higher cellulose loading would cause higher polarizability arising from the increased number of —OH groups in the composite. Several reports showed similar effects due to increased

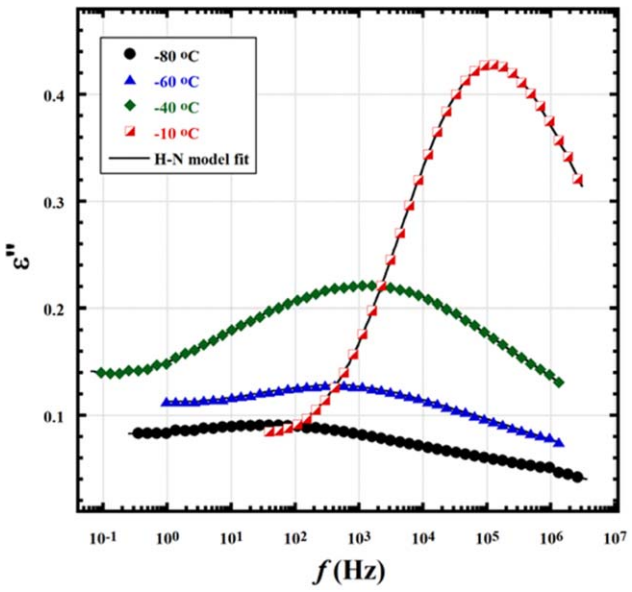

Figure 13. ε'' vs. f spectra for the control electrospun PVDF within the β-relaxation temperature range. Lines represent the HN equation fits to the spectra. [Color figure can be viewed in the online issue, which is available at wileyonlinelibrary.com.]

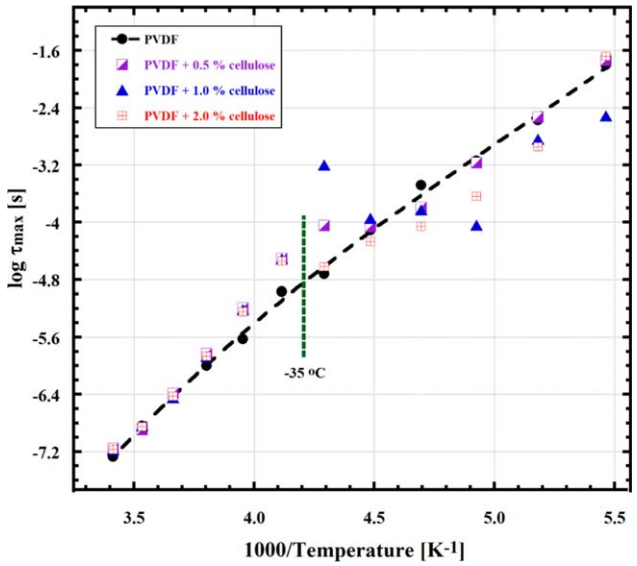

Figure 14. VFTH plots for the β-relaxation of the control and the PVDF/cellulose composites. The dashed line represents the VFTH equation fit to the data for the PVDF control sample. [Color figure can be viewed in the online issue, which is available at wileyonlinelibrary.com.]

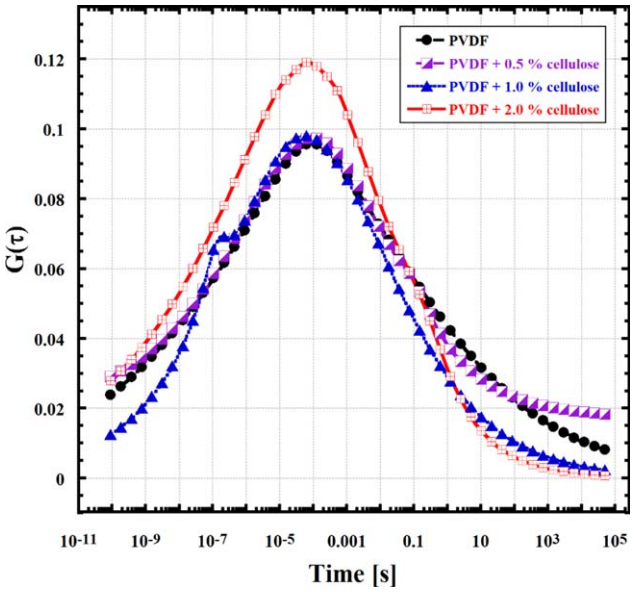

Figure 15. Distributions of relaxation times at −50 °C for the electrospun PVDF/cellulose samples. [Color figure can be viewed in the online issue, which is available at wileyonlinelibrary.com.]

fullerene concentration in thiolene and urethane nanocomposite polymer networks.[42,43] Another possible reason could result from the abovementioned observation of decreased diameters of the produced (nano)fibers with increasing cellulose concentration. Reduction in the diameters would cause better chain packing, and would therefore increase the dipole density which would contribute to the increase in ε'. Similar to our observation herein, Gregorio and Ueno reported that uniaxial drawing of PVDF films could induce better chain packing and increased dipole density, thus increasing the ε' values.[32]

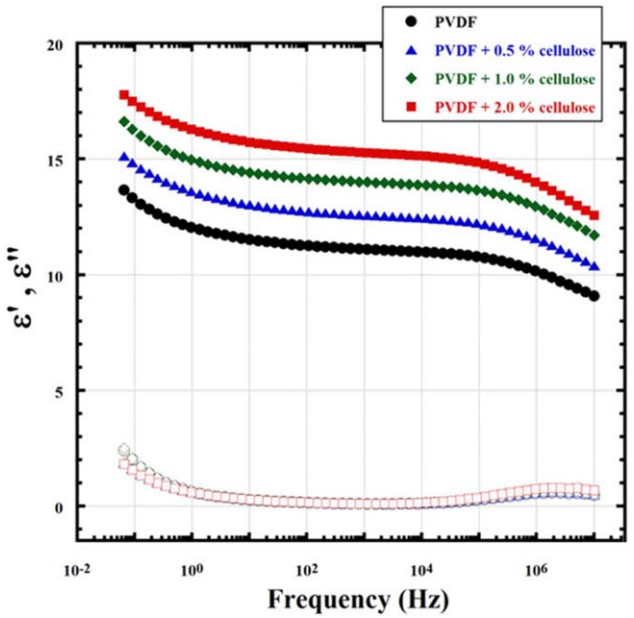

Figure 16. Dielectric permittivity storage (closed symbols) and loss (open symbols) of the electrospun PVDF/cellulose composite films having different compositions at 20 °C. [Color figure can be viewed in the online issue, which is available at www.interscience.wiley.com.]

The drop in the ε' values at lower f (Figure 16) is most probably due to Maxwell–Wagner–Sillars (MWS) interfacial polarization[44] and electrode polarization effects,[42] while the drop at higher f is due to the above-illustrated β-relaxation dispersion. One interesting feature shown in Figure 16 is the higher values of ε' over ε'', supporting that these composites may prove desirable for energy storage media applications.[45] The maximum electrical energy storage capacity ($U_{max} = \varepsilon' E_b^2/2$) require both large ε' and high dielectric breakdown strength (E_b) to achieve large electrical energy storage.[45]

CONCLUSIONS

This investigation looked at the possibility of improving the β-phase content and degree of crystallinity of PVDF through electrospinning of PVDF mixed with small amounts of cellulose. One would expect interactions between the hydroxyl groups on the cellulose and the fluorine atoms in PVDF, which would force the fluorine atoms in PVDF to be in the trans-conformation. The cellulose particles could then act as nucleation centers that would encourage the formation of β-crystals during PVDF crystallization, especially when being electrospun. Electrospinning was used to prepare the PVDF/cellulose (nano)-fibrous films, but it was found that although the total crystallinity and the formation of β-crystals were improved, these improvements were mainly brought about by the chain- and crystal orientation as a result of electrospinning with very little additional contribution from the cellulose dispersed in the electrospun PVDF. However, it was found that the thermal stability of PVDF in the composites slightly increased with increasing cellulose content in the composites up to 1.0 wt %, while the modulus and tensile strength significantly increased up to the same filler level. Broadband dielectric analysis of the PVDF/cellulose composites revealed that the β-relaxation dynamics, assigned to the long-range motions and accounting for the chain segments activity within the crystalline–amorphous interphase, did not change with cellulose insertion. The same was evident for the γ-relaxation, which accounts for the short-range local motions of the chains in the amorphous region. The higher values of ε' over ε'' at room temperature for the composites suggest that they could be useful for energy storage applications such as supercapacitors.

REFERENCES

1. Martins, P.; Lopes, A. C.; Lanceros-Mendez, S. *Progr. Polym. Sci.* **2014**, *39*, 683.
2. Salimi, A.; Yousefi, A. A. *Polym. Test.* **2003**, *22*, 699.
3. Verma, V.; Rajesh, P. S. M.; Bodkhe, S.; Kamle, S. *TMS Ann. Meeting* **2014**, 35.
4. Rajesh, P. S. M.; Bodkh, S.; Kamle, S.; Verma, V. *Electron. Mater. Lett.* **2014**, *10*, 315.
5. Gregorio, R. *J. Appl. Polym. Sci.* **2006**, *100*, 3272.
6. Benz, M.; Euler, W. B. *J. Appl. Polym. Sci.* **2003**, *89*, 1093.

7. Yee, W. A.; Kotaki, M.; Liu, Y.; Lu, X. *Polymer* **2007**, *48*, 512.
8. El-Zatahry, A. A.; AL-Enizi, A. M.; Abdullah, A. M.; AlMaadeed, M. A.; Wang, J.; Zhao, D.; Al-Deyab, S. *Carbon* **2014**, *71*, 276.
9. Shehata, N.; Madi, N.; Al-Maadeed, M.; Hassounah, I.; Ashraf, A. *J. Nanomater.* **2015**, *2015*, 812481.
10. Matabola, K. P.; Moutloali, R. M. *J. Mater. Sci.* **2013**, *48*, 5475.
11. Achaby, M. E.; Arrakhiz, F. Z.; Vaudreuil, S.; Essassi, E. M.; Qaiss, A. *Appl. Surf. Sci.* **2012**, *258*, 7668.
12. Bodkhe, S.; Rajesh, P. S. M.; Kamle, S.; Verma, V. *J. Polym. Res.* **2014**, *21*, 1.
13. Low, Y. K. A.; Tan, L. Y.; Tan, L. P.; Boey, F. Y. C.; Ng, K. W. *J. Appl. Polym. Sci.* **2013**, *128*, 2902.
14. Kamide, K.; Okajima, K.; Matsui, T.; Manabe, S. I. *Polym. J.* **1980**, *12*, 521.
15. Yuan, J.; Geng, J.; Xing, Z.; Shen, J.; Kang, I. K.; Byun, H. *J. Appl. Polym. Sci.* **2010**, *116*, 668.
16. Zhang, F.; Ma, X.; Cao, C.; Li, J.; Zhu, Y. *J. Power Sources* **2014**, *251*, 423.
17. Truong, Y. B.; O'Bryan, Y.; McKelvie, I. D.; Kyratzis, I. L.; Humphries, W. *Macromol. Mater. Eng.* **2013**, *298*, 590.
18. AlMaadeed, M. A.; Ouederni, M.; Khanam, P. N. *Mater. Des.* **2013**, *47*, 725.
19. Al-Ma'adeed, M. A.; Al-Qaradawi, I. Y.; Madi, N.; Al-Thani, N. J. *Appl. Surf. Sci.* **2006**, *252*, 3316.
20. Nallasamy, P.; Mohan, S. *Indian J. Pure Appl. Phys.* **2005**, *43*, 821.
21. Lanceros-Méndez, S.; Mano, J. F.; Costa, A. M.; Schmidt, V. H. *J. Macromol. Sci. B* **2001**, *40*, 517.
22. An, N.; Liu, S.; Fang, C.; Yu, R.; Zhou, X.; Cheng, Y. *J. Appl. Polym. Sci.* **2015**, *132*, 1.
23. Layek, R. K.; Das, A. K.; Park, M. J.; Kim, N. H.; Lee, J. H. *Carbon* **2015**, *81*, 329.
24. Tawansi, A.; Oraby, A. H.; Badr, S. I. I. S. *Polym. Int.* **2004**, *53*, 370.
25. Botelho, G.; Lanceros-Mendez, S.; Gonçalves, A. M.; Sencadas, V.; Rocha, J. G. *J. Noncrystalline Solids* **2008**, *354*, 72.
26. C. L. Beyler, M. M. Hirschler., Thermal decomposition of polymers. SFPE Handbook of Fire Protection Engineering 2, Section 1, Chapter 7, p. 111-131, Springer, **2002**.
27. Arseneau, D. F. *Can. J. Chem.* **1971**, *49*, 632.
28. Feng, Y.; Wang, B.; Wang, F.; Zhao, Y.; Liu, C.; Chen, J.; Shen, C. *Polym. Degrad. Stab.* **2014**, *107*, 129.
29. Luyt, A. S. *eXPRESS Polym. Lett.* **2015**, *9*, 756.
30. Zhang, X.; Feng, J.; Liu, X.; Zhu, J. *Carbohydr. Polym.* **2012**, *89*, 67.
31. A. Schönhals., In Broadband Dielectric Spectroscopy; Kremer, F.; Schönhals, A., Eds.; Springer: Berlin, Heidelberg, **2003**; p 225.
32. Gregorio, R.; Ueno, E. M. *J. Mater. Sci.* **1999**, *34*, 4489.
33. Hahn, B.; Wendorff, J.; Yoon, D. Y. *Macromolecules* **1985**, *18*, 718.
34. Ando, Y.; Hanada, T.; Saitoh, K. *J. Polym. Sci. B: Polym. Phys.* **1994**, *32*, 179.
35. Sencadas, V.; Lanceros-Mendez, S.; Sabater i Serra, R.; Andrio Balado, A.; Gomez Ribelles, J. L. *Eur. Phys. J. E* **2012**, *35*, 41.
36. Nakagawa, K.; Ishida, Y. *J. Polym. Sci. B: Polym. Phys.* **1973**, *11*, 1503.
37. Yagi, T.; Tatemoto, M.; Sako, J. *Polym. J.* **1980**, *12*, 209.
38. S. Havriliak, S. Negami., *J. Polym. Sci. Polym. Symp.* **1966**, *14*, 99.
39. Havriliak, S.; Negami, S. *Polymer* **1967**, *8*, 161.
40. Vogel, S. *Physikalische Zeitschrift* **1921**, *22*, 645.
41. Fulcher, G. S. *J. Am. Ceram. Soc.* **1925**, *8*, 339.
42. Tammann, G.; Hesse, W. *Zeitschrift für anorganische und allgemeine Chemie* **1926**, *156*, 245.
43. Liu, Z.; Maréchal, P.; Jérôme, R. *Polymer* **1997**, *38*, 4925.
44. Ahmed, H. M.; Hassan, M. K.; Mauritz, K. A.; Bunkley, S. L.; Buchanan, R. K.; Buchanan, J. P. *J. Appl. Polym. Sci.* **2014**, *131*, 40577.
45. Ahmed, H. M.; Windham, A. D.; Al-Ejji, M. M.; Al-Qahtani, N. H.; Hassan, M. K.; Mauritz, K. A.; Buchanan, R. K.; Buchanan, J. P. *Materials* **2015**, *8*, 7795.
46. Vasundhara, K.; Mandal, B. P.; Tyagi, A. K. *RSC Adv.* **2015**, *5*, 8591.
47. Li, J.; Zhang, L.; Ducharme, S. *Appl. Phys. Lett.* **2007**, *90*, 132901.